

CrossView-GS: Cross-view Gaussian Splatting For Large-scale Scene Reconstruction

Chenhao Zhang, Yuanping Cao and Lei Zhang*, *Member, IEEE*,

Abstract—3D Gaussian Splatting (3DGS) has emerged as a prominent method for scene representation and reconstruction, leveraging densely distributed Gaussian primitives to enable real-time rendering of high-resolution images. While existing 3DGS methods perform well in scenes with minor view variation, large view changes in cross-view scenes pose optimization challenges for these methods. To address these issues, we propose a novel cross-view Gaussian Splatting method for large-scale scene reconstruction, based on dual-branch fusion. Our method independently reconstructs models from aerial and ground views as two independent branches to establish the baselines of Gaussian distribution, providing reliable priors for cross-view reconstruction during both initialization and densification. Specifically, a gradient-aware regularization strategy is introduced to mitigate smoothing issues caused by significant view disparities. Additionally, a unique Gaussian supplementation strategy is utilized to incorporate complementary information of dual-branch into the cross-view model. Extensive experiments on benchmark datasets demonstrate that our method achieves superior performance in novel view synthesis compared to state-of-the-art methods.

Index Terms—Novel View Synthesis, 3D Gaussian Splatting, Large-scale Scene Reconstruction.

I. INTRODUCTION

3D Gaussian Splatting (3DGS) represents 3D scenes through the use of densely distributed Gaussian primitives, enabling the real-time rendering of high-resolution and high-quality images. It has increasingly become a prevalent method for scene representation. In recent years, with the rapid advancement of sensors and the proliferation of unmanned devices, it has become feasible to capture large-scale scenes with cross-view data at a low cost using drones and mobile phones. Cross-view data [2] collected from aerial and ground views offers a comprehensive approach, with aerial views providing broad coverage and ground views focusing on fine details, thereby enabling the comprehensive reconstruction of complex scenes. This technology holds significant application value in fields such as virtual reality, smart cities, and geographic information systems, *etc.*

However, existing methods for reconstruction based on 3DGS typically assume that the input images come from a set of views that cover the surroundings of the scene, which have relatively stable changes of views and achieve Adaptive Densification Control (ADC) by calculating the average gradient from randomly selected views within the fixed steps [3]. Actually, significant differences in views can lead to issues with ADC [4], [5]. When reconstructing based

on cross-view images, the salient gradients in a certain view may be excessively smoothed by other views with large changes, which can affect the densification effect in areas of significant gradient. This ultimately results in incomplete reconstruction outcomes, which may even be inferior to those achieved using the individual views. [6] uses 3DGS based on aerial views to iteratively extrapolate, generating lower-altitude views to approximate ground views, thus achieving cross-view registration and reconstruction. However, this method requires manually pre-specifying a series of camera poses at intermediate altitudes for each scene and relies on the assumption that the novel view synthesis based on perceptual regularization functions is highly robust, significantly increasing the reconstruction difficulty. Furthermore, the problem of how to effectively utilize complementary information from cross-view data for reconstruction remains insufficiently explored.

Classic methods [7]–[9] based on cross-view data typically employ the Siamese-like architecture. This design extracts information separately from aerial and ground views to establish two branches, fusing information between branches to accomplish downstream tasks in cross-view scenarios. This methodology effectively navigates the challenges posed by substantial differences between aerial and ground views while fully leveraging the unique information inherent in them. Inspired by this approach, we employ the dual-branch models that are reconstructed separately to establish the baseline of Gaussian distributions for aerial and ground views. These distributions provide reliable priors that guide the optimization of cross-view reconstruction during both the initialization and densification processes, addressing the optimization challenges presented by significant view variations in cross-view data and enabling a comprehensive reconstruction of large-scale scenes.

The main contribution of this work is the proposal of a cross-view-based large-scale scene reconstruction method achieved through dual-branch fusion. We first construct dual branches based on aerial and ground views as priors, providing point clouds for initialization in cross-view reconstruction. Gradient-aware regularization are then applied during the reconstruction process. Subsequently, we further integrate complementary information through the unique Gaussians supplementation method. We extensively validate our contributions on representative scenes from benchmark datasets such as MatrixCity [10], UC-GS [5], and ISPRS [11]. Experimental results demonstrate that our proposed method effectively addresses the optimization challenges of 3DGS in cross-view reconstruction and outperforms previous works in novel view synthesis.

Chenhao Zhang, Yuanping Cao and Lei Zhang are with the School of Computer Science, Beijing Institute of Technology, Beijing 100081, China.

* Corresponding author: leizhang@bit.edu.cn



Fig. 1. **Left:** Compared to Scaffold-GS [1], our method achieves better rendering quality on the cross-view NYC scene. **Right:** The plot shows that the SOTA methods encounter difficulties in optimizing the cross-view scene, resulting in performance degradation compared to separate reconstruction based on two individual views. Our method overcomes the challenge of large view changes and surpasses the SOTA methods in quantitative evaluation like PSNR.

II. RELATED WORK

There are numerous published approaches for 3D scene reconstruction, and we refer interested readers to [12]–[14] for a comprehensive overview. In this context, we focus on scene reconstruction based on 3DGS and cross-view data that are most relevant to our approach.

A. Reconstruction based on 3DGS

3DGS, with its significant advantages in rendering quality and efficiency, has become one of the most mainstream methods for scene reconstruction. Currently, there are some works attempting to improve the densification strategy in 3DGS. Pixel-GS [15] promotes the densification of large Gaussian primitives by considering the number of pixels covered by the Gaussian in each perspective. [16] proposes using an auxiliary per-pixel error function as the criteria for densification and correcting biases in opacity handling strategies. Although these works have successfully improved the densification strategy of the original 3DGS, none has addressed the gradient smoothing issue caused by abrupt changes in views.

Some studies based on 3DGS have also focused on large-scale scene reconstruction. For example, CityGaussian [17] propose a divide-and-conquer training method and a Level-of-Detail-based real-time rendering strategy, enabling efficient large-scale scene rendering. VastGaussian [18], through a progressive partitioning strategy and appearance-decoupled modeling, achieves rapid optimization and high-fidelity real-time rendering. Hier-GS [19] introduces a hierarchical structure of 3D Gaussians along with a Level-of-Detail scheme, similarly enabling real-time rendering for large-scale scenes. However, these works typically assume a single type of views as input and do not consider the challenges of comprehensive reconstruction caused by cross-view data.

B. Reconstruction based on cross-view data

The concept of cross-view originates from the task of “cross-view image geo-localization” introduced by [2], which typically involves aerial views captured by satellites or drones and ground views collected by vehicles or handheld imaging

devices. The task addressed in this paper is to reconstruct large-scale scenes based on cross-view data composed of aerial and ground views. Traditional cross-view reconstruction methods are generally based on photogrammetry [20], [21]. With the advent of 3DGS, UC-GS [5] proposes leveraging aerial views to assist ground-view reconstruction, thereby improving the performance of autonomous driving. DRAGON [6] extrapolates 3DGS trained on aerial views to iteratively generate lower-altitude views, eventually approximating ground views, enabling view alignment and scene reconstruction. However, first, cross-view registration tasks currently have relatively mature solutions [22]–[25]. Second, DRAGON requires manually setting intermediate camera poses during the iterative extrapolation process, which hinders the deployment and generalization of this approach. Lastly, when setting viewpoints during extrapolation iterations, DRAGON also accounts for the robustness of rendering. Excessive extrapolation results in low-quality novel view synthesis by 3DGS, while limited extrapolation significantly increases computational costs. Our work addresses the optimization of 3DGS in cross-view reconstruction and successfully automates the comprehensive reconstruction of large-scale scenes.

III. METHOD OVERVIEW

We outline the proposed method to establish context for the core algorithm described in the next section. As shown in Fig. 2, our method aims to reconstruct large-scale scenes from a collection of cross-view images captured by drones and ground devices.

Specifically, we first train the dual-branch models independently using aerial and ground views to facilitate cross-view reconstruction, and the structured point clouds are extracted from the aerial model to serve as the initial distribution for cross-view reconstruction. Then, the gradient-aware regularization based on pseudo-labels generated by the dual-branch models is applied to optimize the reconstruction process. Finally, by assessing overlapping regions from the dual-branch models, unique Gaussian primitives are incorporated into the cross-view reconstruction and the final reconstruction is completed through fine-tuning.

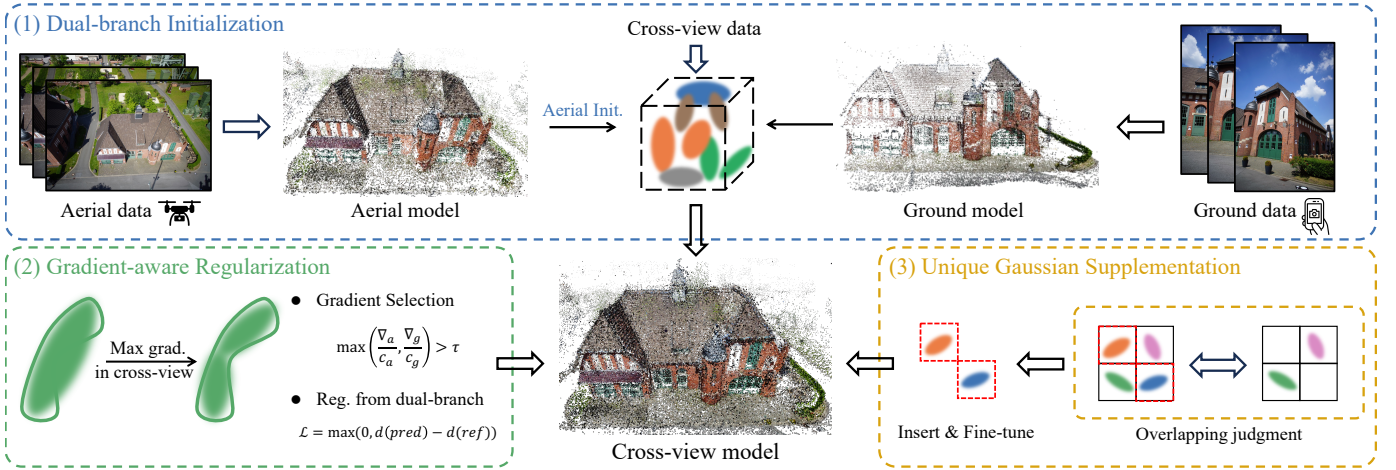


Fig. 2. **An overview of the proposed methodology.** Our method first initializes the dual-branch structure that includes both aerial and ground models. Then, we initialize the cross-view model based on the aerial model and introduce a gradient-sensitive regularization strategy based on dual branches to reconstruct the cross-view model. Finally, we supplement the cross-view model with unique Gaussian primitives based on the dual-branch models, thereby completing the reconstruction of large-scale scenes.

IV. CROSS-VIEW RECONSTRUCTION

We initially establish two branches as priors. Subsequently, we enhance the ADC by leveraging the characteristics of gradients in cross views and fully incorporating unique information from different types of views.

A. Dual-branch initialization

To address the optimization challenges caused by significant view changes, we follow the Siamese-like architecture during the initial stage, using the state-of-the-art 3DGS method Scaffold-GS [1] to reconstruct scenes from aerial and ground views, resulting in the aerial model \mathcal{G}_a and the ground model \mathcal{G}_g . The set of 3D Gaussian primitives is defined as $\mathcal{G} = \{G_i(\mu_i, \Sigma_i, \alpha_i, f_i) \mid i = 1, 2, \dots, N\}$, where μ_i , Σ_i , α_i , and f_i represent the mean, covariance matrix, transparency, and feature vector (RGB color or spherical harmonics) of the i -th Gaussian, respectively.

Initialization based on aerial model. Inspired by PyGS [26], to obtain a more comprehensive structured point cloud for large-scale scenes as the initial distribution, we downsample the Gaussian distribution of the aerial model to generate the point cloud pc . This process can be expressed as:

$$\mathcal{G}' = \text{Downsample}(\mathcal{G}, \tau), \quad (1)$$

where τ is the downsampling ratio. Based on the downsampled Gaussian distribution \mathcal{G}' , the center position μ'_i of each Gaussian primitive G'_i is selected to generate the point cloud as $pc = \cup \mu'_i$. Subsequently, we use pc as the initial point cloud to reconstruct the cross-view model \mathcal{G}_f based on cross-view images.

B. Gradient-aware regularization

Due to significant view differences, 3DGS faces challenges in reconstruction based on cross-view images. Our observations indicate that these challenges mainly stem from the limitations of the densification strategy in ADC. The densification

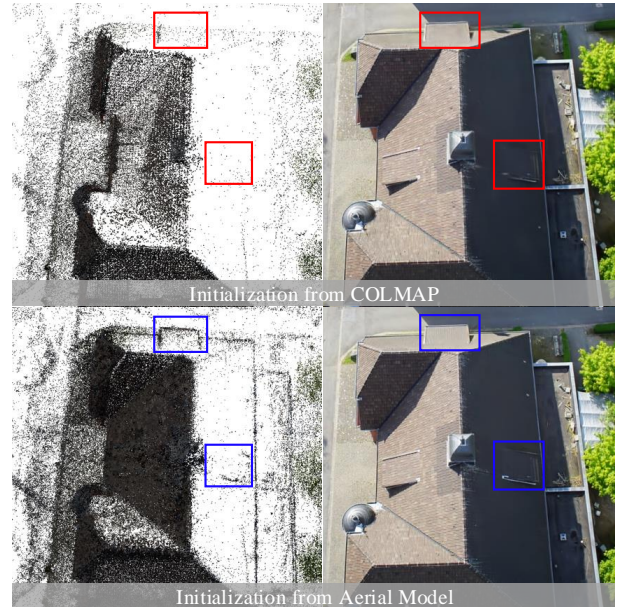


Fig. 3. Point clouds and reconstruction results by different initial methods.

strategy of 3DGS relies on gradient statistics within fixed time steps. Taking Scaffold-GS as an example, for each Gaussian primitive G , the cumulative gradient ∇_π and cumulative visibility count c_π over N training iterations are calculated based on the training camera poses π , and the average gradient is then computed as $\nabla_{avg} = \nabla_\pi / c_\pi$. Next, the set of Gaussian primitives satisfying $\nabla_{avg} > \tau$ is selected, where τ is a predefined threshold denoted by $\mathcal{G}_\pi = \{G \mid \frac{\nabla_\pi}{c_\pi} > \tau\}$. If the voxel space containing the Gaussian primitives \mathcal{G}_π does not already have an anchor, a new anchor is deployed at the center of the voxel, completing the densification process.

With the images of aerial views v_a or ground views v_g , the densified set of Gaussian primitives is

$$\left\{ G \left| \frac{\nabla v}{c_v} > \tau, v \in v_a \vee v \in v_g \right. \right\}. \quad (2)$$

Then, using cross-view images v_f , the densified set of Gaussian primitives is

$$\left\{ G \left| \frac{\nabla f}{c_f} > \tau, f = v_a \cup v_g \right. \right\} = \left\{ G \left| \frac{\nabla_a + \nabla_g}{c_a + c_g} > \tau \right. \right\}. \quad (3)$$

Since the max values of $\frac{\nabla_a + \nabla_g}{c_a + c_g}$, $\frac{\nabla_a}{c_a}$ and $\frac{\nabla_g}{c_g}$ are only equal when $\frac{\nabla_a}{c_a} = \frac{\nabla_g}{c_g}$, the salient gradients for densification are prone to being smoothed out. This leads the model to fall into local optima, preventing it from achieving the same densification effect as in single-view reconstruction (see Fig. 4).

During the training of the cross-view model \mathcal{G}_f , we propose a gradient-aware regularization to alleviate the problem of salient gradients being smoothed out. This regularization strategy consists of two components: an adjustment to the gradient selection criterion for cross-view images and the additional regularization constraints based on the dual-branch models.

Firstly, large view changes may cause inconsistencies in the gradients of Gaussian primitives across different views. To address this issue, we modify the gradient selection criterion in the densification strategy to accommodate cross-view variations. Specifically, to accurately identify Gaussian primitives with salient gradients based on cross-view images and achieve densification effects comparable to single-view construction, we separately record the gradients (∇_a and ∇_g) and visibility counts (c_a and c_g) of Gaussian primitives under aerial and ground views. The densified Gaussian primitive set \mathcal{G}_{cross} is then determined using the maximum gradient from the single type of views:

$$\mathcal{G}_{cross} = \left\{ G \left| \max\left(\frac{\nabla_a}{c_a}, \frac{\nabla_g}{c_g}\right) > \tau \right. \right\} \quad (4)$$

Next, inspired by the triplet loss [27], we use the rendering of the trained dual-branch models under the corresponding views as the pseudo label of regularization. By penalizing regions in the cross-view model where the reconstruction quality is lower than that of the dual-branch models, additional gradients are introduced. Specifically, given a training viewpoint v_t , the rendering of the dual-branch models \mathcal{G}_a and \mathcal{G}_g under the current view are used as the pseudo label ref . An additional loss term penalizes parts of the cross-view model's rendering $pred$ that deviate further from the ground truth gt than pseudo label ref . This process can be expressed as:

$$\mathcal{L}_{reg} = \max(0, d(pred, gt) - d(ref, gt)), \quad (5)$$

where $d()$ is a distance metric function, and $d(ref, gt)$ is the reference distance. This ensures that $pred$ is optimized to be closer to gt than ref , while the $\max()$ function ensures that this loss term is effective only when $pred$ deviates further from gt than ref .

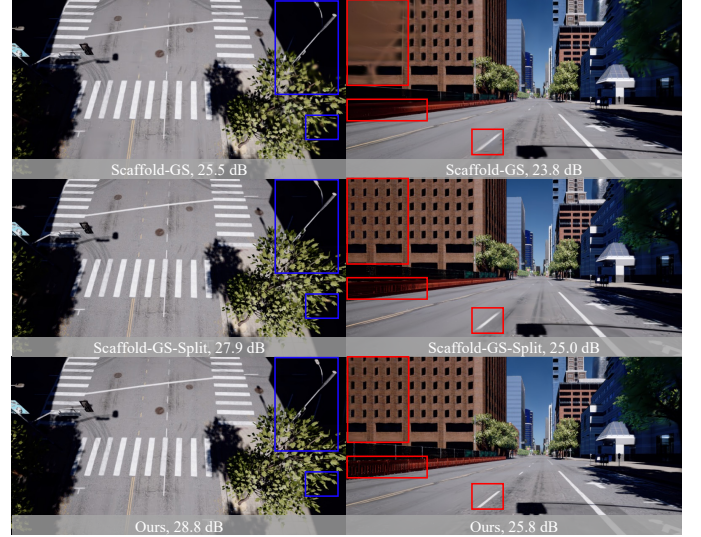
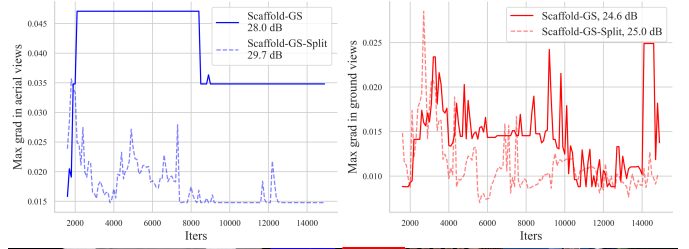


Fig. 4. Gradient smoothing problem caused by cross-view reconstruction. The first row shows the variation of maximum gradient in different views during densification when using cross-view or single-view for reconstruction. The second and third rows represent the result of Scaffold-GS [1] using cross-view data and single-view data, respectively. The last row indicates the result of our CrossView-GS using cross-view data.

C. Unique Gaussian supplementation

To fully integrate complementary information from cross-view images, we determine whether Gaussian primitives in the single models and the cross-view model overlap based on a voxel grid. This approach allows us to identify the densified regions unique to each branch during their respective training processes. Subsequently, these unique Gaussian primitives are incorporated into the cross-view model and further optimized through fine-tuning. Specifically, the dual-branch models (\mathcal{G}_a or \mathcal{G}_g), and the cross-view model \mathcal{G}_f are reconstructed using Scaffold-GS with the same voxel size. The voxel grid represents the valid mask of anchors. Define the voxel grid of the cross-view model as \mathcal{V}_f and those of the dual-branch models as \mathcal{V}_a and \mathcal{V}_g . A Gaussian primitive $G_i \in \mathcal{G}_a \cup \mathcal{G}_g$ is considered to be non-overlapping with the cross-view model if its anchor's corresponding voxel ν_i satisfies $\nu_i \notin \mathcal{V}_f$. Finally, all non-overlapping Gaussian primitives from the dual-branch models are incorporated into the cross-view model, and the updated cross-view model \mathcal{G}_f' is expressed as:

$$\mathcal{G}_f' = \mathcal{G}_f \cup \{G_i \mid G_i \in \mathcal{G}_a \cup \mathcal{G}_g, \nu_i \notin \mathcal{V}_f\}. \quad (6)$$

Considering that neural Gaussians in Scaffold-GS possess implicit attributes related to MLPs (e.g., color and opacity), a small iterations of fine-tuning are required for the updated

TABLE I
 QUANTITATIVE EVALUATION OF THE PROPOSED METHOD AND SOTA METHODS WITH BLOCK_SMALL SCENE IN MATRIXCITY [10], ZECHÉ SCENE IN ISPRS [11], NYC AND SF SCENES IN UC-GS [5]. WE HIGHLIGHT THE BEST AND SECOND-BEST ONES IN EACH CATEGORY.

Method		Scene		Block_small in MatrixCity			Zeche in ISPRS						
				All			Aerial	Ground	All			Aerial	Ground
				PSNR \uparrow	SSIM \uparrow	LPIPS \downarrow	PSNR \uparrow	PSNR \uparrow	PSNR \uparrow	SSIM \uparrow	LPIPS \downarrow	PSNR \uparrow	PSNR \uparrow
I-NGP	SIG. 2022	19.177	0.585	0.588	17.408	19.649	18.294	0.475	0.637	17.859	18.649		
3DGS	SIG. 2023	22.998	0.787	0.304	21.930	23.283	23.344	0.764	0.274	23.006	23.619		
Scaffold-GS	CVPR 2024	24.081	<u>0.813</u>	0.270	<u>26.493</u>	23.437	<u>24.606</u>	<u>0.792</u>	<u>0.250</u>	<u>24.531</u>	<u>24.668</u>		
Hier-GS	SIG. 2024	<u>24.410</u>	<u>0.813</u>	<u>0.267</u>	26.381	<u>23.885</u>	23.050	0.748	0.279	22.740	23.304		
CrossView-GS		25.233	0.846	0.213	28.464	24.371	25.322	0.818	0.214	25.476	25.196		
Method		Scene		NYC in UC-GS			SF in UC-GS						
				All			Aerial	Ground	All			Aerial	Ground
				PSNR \uparrow	SSIM \uparrow	LPIPS \downarrow	PSNR \uparrow	PSNR \uparrow	PSNR \uparrow	SSIM \uparrow	LPIPS \downarrow	PSNR \uparrow	PSNR \uparrow
I-NGP	SIG. 2022	20.390	0.546	0.489	21.219	19.561	22.162	0.504	0.535	22.924	21.399		
3DGS	SIG. 2023	26.087	0.818	0.258	27.395	24.778	26.648	0.758	0.314	28.691	24.605		
Scaffold-GS	CVPR 2024	26.622	0.812	0.250	27.960	25.284	26.305	0.730	0.354	28.037	24.574		
Hier-GS	SIG. 2024	<u>27.617</u>	<u>0.837</u>	0.200	<u>29.157</u>	<u>26.076</u>	27.633	0.784	<u>0.281</u>	<u>29.635</u>	25.631		
CrossView-GS		28.066	0.841	<u>0.203</u>	29.794	26.338	<u>27.592</u>	<u>0.777</u>	0.279	29.894	<u>25.290</u>		

cross-view model $\mathcal{G}_{f'}$. This ensures that the supplemented Gaussian primitives correctly decode appearance information.

Loss design. We basically follow the design of Scaffold-GS [1], using the loss function \mathcal{L}_s composed of per-pixel color loss \mathcal{L}_1 , SSIM term [28] \mathcal{L}_{SSIM} , and volume regularization [29] \mathcal{L}_{vol} . In the fine-tune phase, we use the loss function \mathcal{L}_s , which is given by:

$$\mathcal{L}_s = \mathcal{L}_1 + \lambda_{SSIM}\mathcal{L}_{SSIM} + \lambda_{vol}\mathcal{L}_{vol}, \quad (7)$$

In addition, we also introduce the gradient-aware regularization term \mathcal{L}_{reg} during the first training of cross-view model to penalize regions with lower rendering quality than the dual-branch models. The total loss function \mathcal{L} is expressed as:

$$\mathcal{L} = \lambda_{reg}\mathcal{L}_{reg} + \mathcal{L}_s, \quad (8)$$

V. EXPERIMENTS

We have implemented novel view synthesis using the proposed CrossView-GS, and carried out comprehensive evaluations in rendering quality. We also compare our method with state-of-the-art (SOTA) methods, like Instant-NGP [30], 3DGS [3], Scaffold-GS [1] and Hier-GS [19]. For fair comparison, we all use the default training epochs of SOTA methods. For Hier-GS, we report the rendering quality of its leaves. As done by SOTA methods, we used Block_small scene in MatrixCity dataset [10], NYC and SF in UC-GS dataset [5] and real captured Zeche scene in ISPRS dataset [11] for evaluation. For the UC-GS dataset [5], we utilize the scene captured at an aerial altitude of 20 meters and a ground altitude of 1.5 meters. To better evaluate the reconstruction of cross-view scenes, the dataset is re-divided into training and test sets by selecting one test image out of every eight, based on the image suffix number. Next, we elaborate the details of the experiments.

A. Implementations

We basically follow the settings of Scaffold-GS [1]. We train the dual-branch models and the cross-view model with 30k iterations. Then, we implement unique Gaussian supplementation to cross-view model and finetune it for 20k iterations. The downscale rate τ is set to 10. For the loss function, parameters λ_{SSIM} , λ_{vol} and λ_{reg} are set to 0.2, 0.01 and 1.0. It takes about 70 minutes to complete our reconstruction on Zeche in ISPRS dataset [11]. All experiments are conducted on NVIDIA A6000 GPU with 48G memory.

B. Comparisons

We conduct both quantitative and qualitative evaluation of rendering quality for view synthesis obtained by the proposed method and SOTA methods. Quantitative evaluation uses the metrics of PSNR, SSIM [28] and LPIPS [31] for the assessment of rendering quality. The results of these evaluations are presented in Tab. I.

Compared to other SOTA methods, CrossView-GS demonstrates superior rendering quality in nearly all scenes across both aerial and ground views. Specifically, compared to our baseline Scaffold-GS, CrossView-GS achieves consistent improvements in all scenes, with an average PSNR increase of 1.15 dB. Notably, the quality improvement in aerial views is more pronounced than in ground views, likely because aerial views are more affected by gradient smoothing issues, as illustrated in Fig. 4. Hier-GS achieves exceptional quality in detail-rich ground views, particularly in the SF scene, due to its Level-of-Detail (LoD) structure with strong detail-capturing capability. In contrast, our method delivers competitive performance in ground views across other scenes.

Qualitative comparisons with SOTA methods like Scaffold-GS [1] and Hier-GS [19] are illustrated in Fig. 5 and Fig. 8, where two views are selected for local magnification to highlight differences. Scaffold-GS suffers from significant blurring caused by insufficient densification, particularly in

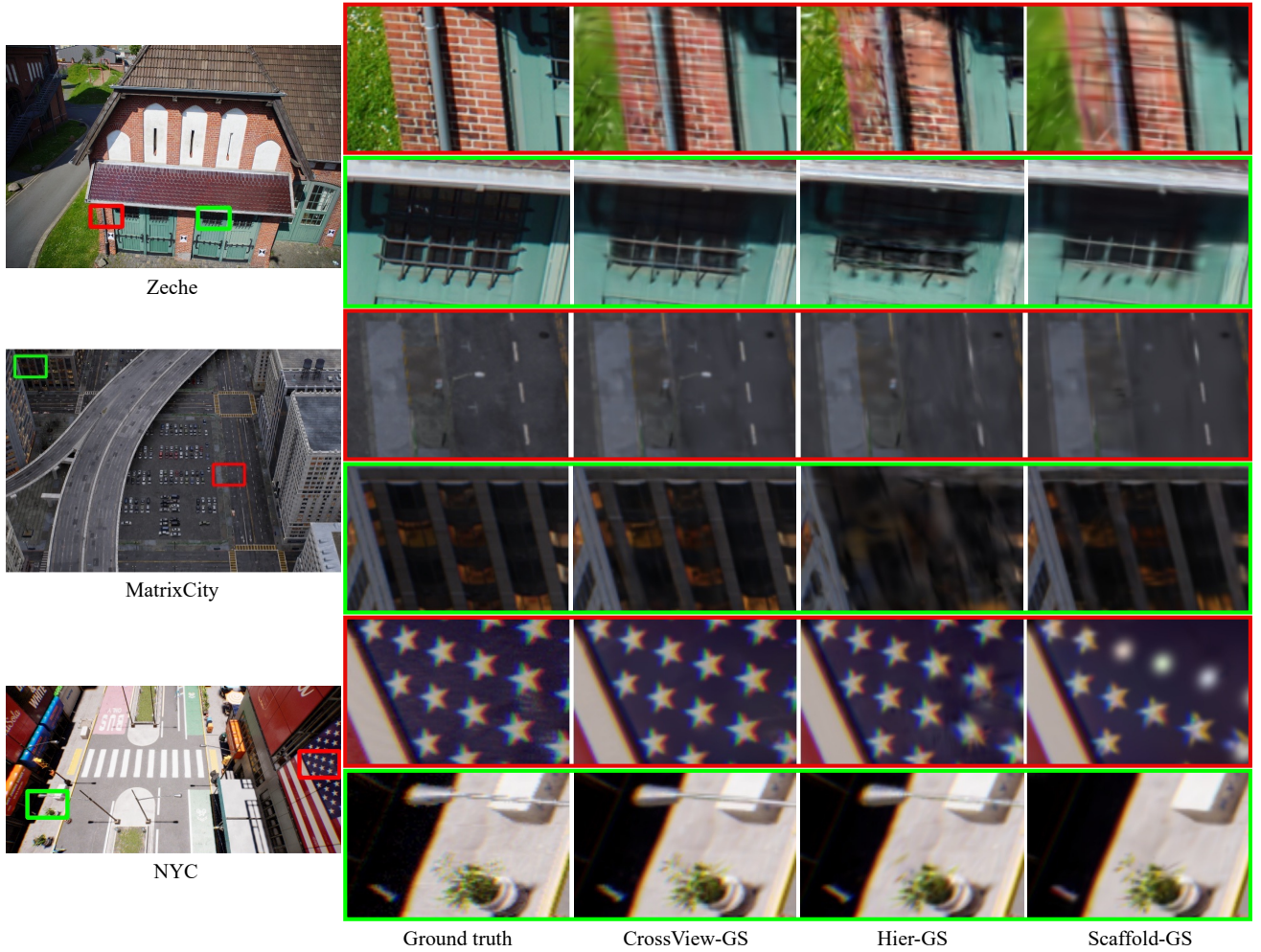


Fig. 5. The rendering results and zoomed-in images obtained by our method CrossView-GS, as well as some SOTA methods.

TABLE II
THE ABLATION STUDY IN THE COMPONENTS OF CROSSVIEW-GS ON NYC
AND SF SCENES OF UC-GS DATASET [5].

Variants	All			Aerial PSNR	Ground PSNR
	PSNR	SSIM	LPIPS		
Baseline	26.464	0.771	0.302	27.998	24.929
w/ Init.	26.814	0.780	0.292	28.592	25.037
w/ Grad.	27.241	0.791	0.263	29.184	25.299
w/ Supp.	27.174	0.792	0.272	28.971	25.377
w/ Init. & Grad.	27.457	0.797	0.257	29.505	25.409
w/ Init. & Supp.	27.333	0.796	0.266	29.242	25.425
Ours	27.829	0.809	0.241	29.844	25.814

aerial views. While Hier-GS exhibits high-quality ground view rendering, its performance in aerial views is not good. In contrast, our method provides more comprehensive rendering results across both aerial and ground views.

C. Ablation study

We conduct ablation experiments on three components of the proposed method on NYC and SF scenes of UC-GS dataset [5], as shown in Tab. II. The assessment is based

on quantitative quality comparisons using PSNR, SSIM, and LPIPS. Meanwhile, we take two views with the same horizontal projection position but different heights and angles as examples to demonstrate the ablation of different components, as shown in Fig. 6.

We first conduct experiments by adding various components based on baseline Scaffold-GS [1] to demonstrate their effectiveness, as shown in the first four rows in Tab. II. It can be seen that the gradient-aware regularization can achieve the maximum performance gain. The point cloud extracted based on aerial views provides rough structural information, improving the quality of aerial views, as shown in the second column in Fig. 6. Based on the third column, we believe that the gradient-aware regularization strategy effectively solves the gradient smoothing problem mentioned in Fig. 4, significantly improving the rendering quality of aerial views. In contrast, the unique Gaussian supplementation achieves more performance improvement from the ground views by combining complementary information from both branches, as shown in the fourth column of the Fig 6. Next, we add two additional components based on the proposed initialization method, both of which achieve further performance improvements. In the end, we achieve the best results of novel view synthesis by



Fig. 6. Qualitative ablations. **Column 1:** The results of Scaffold-GS in cross-view reconstruction. **Column 2:** The results of baseline with initialization from aerial views. **Column 3:** The results of baseline with gradient-aware regularization. **Column 4:** The results of baseline with unique Gaussian supplementation.

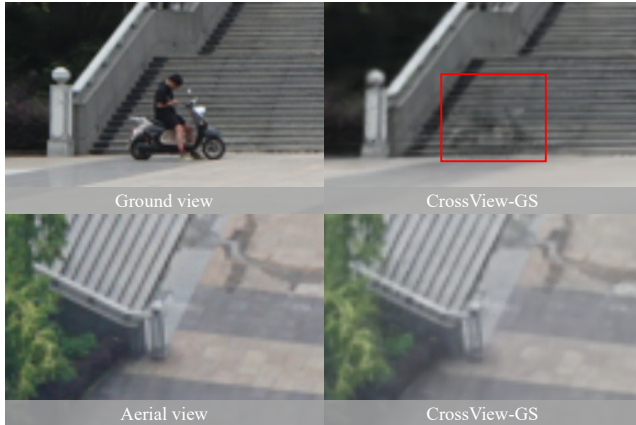


Fig. 7. The cross-view inconsistency caused by dynamic objects results in unnatural artifacts.

combining these three components.

D. Limitations

Although our method can effectively reconstruct large-scale scenes using cross-view data, it is not without limitations. Specifically, our method does not consider dynamic objects in the scene, such as vehicles and pedestrians. The presence of such objects in cross-view data introduces additional spatial ambiguity, as shown in Fig. 7. While predicting masks for moving objects, as employed by Hier-GS, could be a potential solution, its feasibility from the aerial views remains uncertain.

VI. CONCLUSION

We propose the CrossView-GS based on cross-view data for large-scale scene reconstruction. We construct the dual-branch models as a prior by separately reconstructing aerial

and ground views, effectively guiding the optimization of cross-view 3DGS and achieving high-quality reconstruction of large-scale scenes. Experimental evidence demonstrates that our approach outperforms state-of-the-art methods. As the future work, we plan to incorporate the Divide-and-Conquer approach to enable the reconstruction of extremely large-scale scenes using cross-view data.

REFERENCES

- [1] T. Lu, M. Yu, L. Xu, Y. Xiangli, L. Wang, D. Lin, and B. Dai, "Scaffold-gs: Structured 3d gaussians for view-adaptive rendering," in *Proceedings of CVPR*, 2024.
- [2] T.-Y. Lin, S. Belongie, and J. Hays, "Cross-view image geolocalization," in *Proceedings of CVPR*, 2013.
- [3] B. Kerbl, G. Kopanas, T. Leimkühler, and G. Drettakis, "3d gaussian splatting for real-time radiance field rendering," *ACM Transactions on Graphics (TOG)*, vol. 42, no. 4, pp. 1–14, 2023.
- [4] X. Du, Y. Wang, and X. Yu, "Mvgs: Multi-view-regulated gaussian splatting for novel view synthesis," 2024.
- [5] S. Zhang, B. Ye, X. Chen, Y. Chen, Z. Zhang, C. Peng, Y. Shi, and H. Zhao, "Drone-assisted road gaussian splatting with cross-view uncertainty," *arXiv preprint arXiv:2408.15242*, 2024.
- [6] Y. Ham, M. Michalkiewicz, and G. Balakrishnan, "Dragon: Drone and ground gaussian splatting for 3d building reconstruction," in *Proceedings of ICIP*, 2024.
- [7] Y. Shi, L. Liu, X. Yu, and H. Li, "Spatial-aware feature aggregation for image based cross-view geo-localization," 2019.
- [8] S. Hu, M. Feng, R. M. H. Nguyen, and G. H. Lee, "Cvm-net: Cross-view matching network for image-based ground-to-aerial geo-localization," in *Proceedings of CVPR*, 2018.
- [9] K. Regmi and M. Shah, "Bridging the domain gap for ground-to-aerial image matching," in *Proceedings of ICCV*, 2019.
- [10] Y. Li, L. Jiang, L. Xu, Y. Xiangli, Z. Wang, D. Lin, and B. Dai, "Matrixcity: A large-scale city dataset for city-scale neural rendering and beyond," in *Proceedings of ICCV*, 2023.
- [11] F. Nex, M. Gerke, F. Remondino, H.-J. Przybilla, M. Bäumker, and A. Zurhorst, "Isprs benchmark for multi-platform photogrammetry," *ISPRS Annals of the Photogrammetry, Remote Sensing and Spatial Information Sciences*, vol. 2, pp. 135–142, 2015.
- [12] T. Wu, Y.-J. Yuan, L.-X. Zhang, J. Yang, Y.-P. Cao, L.-Q. Yan, and L. Gao, "Recent advances in 3d gaussian splatting," *Computational Visual Media*, vol. 10, no. 4, pp. 613–642, 2024.

- [13] B. Fei, J. Xu, R. Zhang, Q. Zhou, W. Yang, and Y. He, “3d gaussian splatting as new era: a survey,” *IEEE Transactions on Visualization and Computer Graphics*, pp. 1–20, 2024.
- [14] K. Gao, Y. Gao, H. He, D. Lu, L. Xu, and J. Li, “Nerf: Neural radiance field in 3d vision, a comprehensive review,” *arXiv preprint arXiv:2210.00379*, 2022.
- [15] Z. Zhang, W. Hu, Y. Lao, T. He, and H. Zhao, “Pixel-gs: Density control with pixel-aware gradient for 3d gaussian splatting,” in *European Conference on Computer Vision*, 2024.
- [16] S. Rota Bulò, L. Porzi, and P. Kontschieder, “Revising densification in gaussian splatting,” in *Proceedings of ECCV*, 2024.
- [17] Y. Liu, C. Luo, L. Fan, N. Wang, J. Peng, and Z. Zhang, “Citygaussian: Real-time high-quality large-scale scene rendering with gaussians,” in *Proceedings of ECCV*, 2024.
- [18] J. Lin, Z. Li, X. Tang, J. Liu, S. Liu, J. Liu, Y. Lu, X. Wu, S. Xu, Y. Yan, and W. Yang, “Vastgaussian: Vast 3d gaussians for large scene reconstruction,” in *Proceedings of CVPR*, 2024.
- [19] B. Kerbl, A. Meuleman, G. Kopanas, M. Wimmer, A. Lanvin, and G. Drettakis, “A hierarchical 3d gaussian representation for real-time rendering of very large datasets,” *ACM Transactions on Graphics (TOG)*, vol. 43, no. 4, pp. 1–15, 2024.
- [20] X. Gao, S. Shen, Z. Hu, and Z. Wang, “Ground and aerial meta-data integration for localization and reconstruction: A review,” *Pattern Recognition Letters*, vol. 127, pp. 202–214, 2019.
- [21] R. Qin, S. Song, X. Ling, and M. Elhashash, “3d reconstruction through fusion of cross-view images,” *Recent Advances in Image Restoration with Applications to Real World Problems*, p. 123, 2020.
- [22] Q. Zhu, Z. Wang, H. Hu, L. Xie, X. Ge, and Y. Zhang, “Leveraging photogrammetric mesh models for aerial-ground feature point matching toward integrated 3d reconstruction,” *ISPRS Journal of Photogrammetry and Remote Sensing*, vol. 166, pp. 26–40, 2020.
- [23] H. Li, A. Liu, X. Xie, H. Guo, H. Xiong, and X. Zheng, “Learning dense consistent features for aerial-to-ground structure-from-motion,” *IEEE Journal of Selected Topics in Applied Earth Observations and Remote Sensing*, vol. 16, pp. 5089–5102, 2023.
- [24] Z. Hou, Y. Liu, and L. Zhang, “Pos-gift: A geometric and intensity-invariant feature transformation for multimodal images,” *Information Fusion*, vol. 102, p. 102027, 2024.
- [25] J. Liu, H. Yin, B. Liu, and P. Lu, “Tie point matching between terrestrial and aerial images based on patch variational refinement,” *Remote Sensing*, vol. 15, no. 4, 2023. [Online]. Available: <https://www.mdpi.com/2072-4292/15/4/968>
- [26] Z. Wang and D. Xu, “Pygs: Large-scale scene representation with pyramidal 3d gaussian splatting,” 2024.
- [27] F. Schroff, D. Kalenichenko, and J. Philbin, “Facenet: A unified embedding for face recognition and clustering,” in *Proceedings of CVPR*, 2015.
- [28] Z. Wang, A. C. Bovik, H. R. Sheikh, and E. P. Simoncelli, “Image quality assessment: from error visibility to structural similarity,” *IEEE transactions on image processing*, vol. 13, no. 4, pp. 600–612, 2004.
- [29] S. Lombardi, T. Simon, G. Schwartz, M. Zollhoefer, Y. Sheikh, and J. Saragih, “Mixture of volumetric primitives for efficient neural rendering,” *ACM Transactions on Graphics (ToG)*, vol. 40, no. 4, pp. 1–13, 2021.
- [30] T. Müller, A. Evans, C. Schied, and A. Keller, “Instant neural graphics primitives with a multiresolution hash encoding,” *ACM Transactions on Graphics (TOG)*, vol. 41, no. 4, pp. 1–15, 2022.
- [31] R. Zhang, P. Isola, A. A. Efros, E. Shechtman, and O. Wang, “The unreasonable effectiveness of deep features as a perceptual metric,” in *Proceedings of CVPR*, 2018, pp. 586–595.

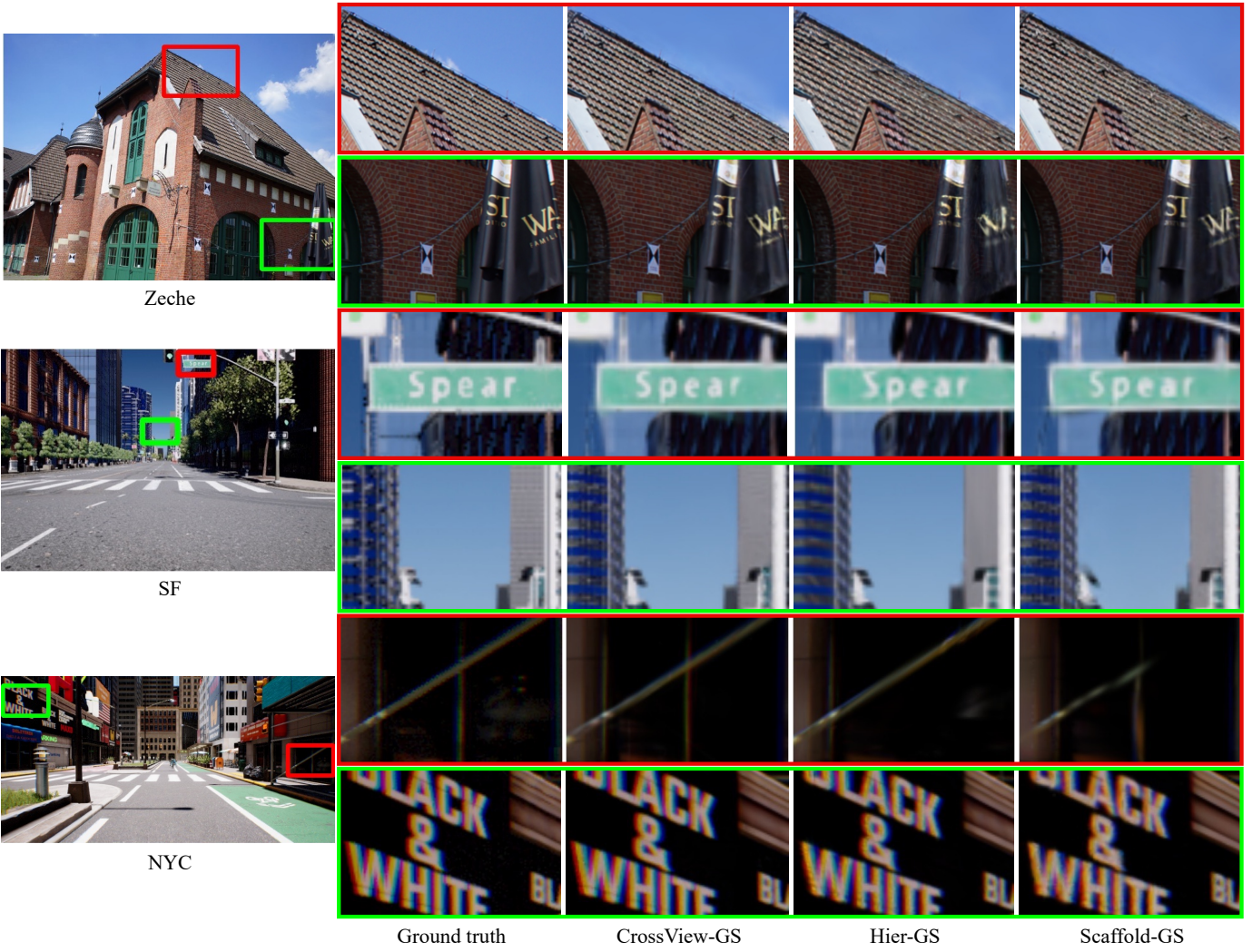


Fig. 8. More rendering results and zoomed-in images obtained by our method, as well as some SOTA methods.